Radiation Driven Chemistry in Biomolecules—is (V)UV Involved in the Bioactivity of Argon Jet Plasmas?

G. Bruno[1,2], S. Wenske[1], H. Mahdikia[3], T. Gerling[1], T. von Woedtke[3,4] and K. Wende[1]*

[1]ZIK Plasmatis, Leibniz Institute for Plasma Science and Technology (INP), Greifswald, Germany, [2]Metabolomics Facility, Berlin Institute of Health (BIH) at Max Delbrück Center for Molecular Medicine, Berlin, Germany, [3]Leibniz Institute for Plasma Science and Technology (INP), Greifswald, Germany, [4]Institute for Hygiene and Environmental Medicine, University Medicine Greifswald, Greifswald, Germany

Cold physical plasmas, especially noble gas driven plasma jets, emit considerable amounts of ultraviolet radiation (UV). Given that a noble gas channel is present, even the energetic vacuum UV can reach the treated target. The relevance of UV radiation for antimicrobial effects is generally accepted. It remains to be clarified if this radiation is relevant for other biomedical application of plasmas, e.g., in wound care or cancer remediation. In this work, the role of (vacuum) ultraviolet radiation generated by the argon plasma jet kINPen for cysteine modifications was investigated in aqueous solutions and porcine skin. To differentiate the effects of photons of different wavelength and complete plasma discharge, a micro chamber equipped with a MgF$_2$, Suprasil, or Borosilicate glass window was used. In liquid phase, plasma-derived VUV radiation was effective and led to the formation of cysteine oxidation products and molecule breakdown products, yielding sulfite, sulfate, and hydrogen sulfide. At the boundary layer, the impact of VUV photons led to water molecule photolysis and formation of hydroxyl radicals and hydrogen peroxide. In addition, photolytic cleavage of the weak carbon-sulfur bond initiated the formation of sulfur oxy ions. In the intact skin model, protein thiol modification was rare even if a VUV transparent MgF$_2$ window was used. Presumably, the plasma-derived VUV radiation played a limited role since reactions at the boundary layer are less frequent and the dense biomolecules layers block it effectively, inhibiting significant penetration. This result further emphasizes the safety of physical plasmas in biomedical applications.

Keywords: cold physical plasma, redox signaling, porcine skin model, VUV radiation, tape stripping model, kINpen

1 INTRODUCTION

Emerging therapies for the treatment of chronic wounds and cancerous lesions involve the administration of exogenous reactive species directly delivered on the target (e.g., cold physical plasmas) [1–4]; or produced *in situ* by administration of specific drugs (e.g., nanoprodrugs) [5,6]. For example, the formation of singlet oxygen by irradiation (600–800 nm) of a photosensitizer, is the molecular mechanism behind the effectiveness of the photodynamic therapy in use for cancer regression [7]. Among the emerging therapies, cold physical plasmas are multi-function tools comprising of reactive species, ions, metastables, electrons, magnetic fields, and photons [8,9]. These, synergistically acting on the target, are effective in cancer regression [10–12]; and wound healing

[13–15]. Furthermore, the use of plasmas is considered in other fields, such as sterilization [16–18]; and dentistry [19–21].

While downstream effects have been detected [11,22], many are the open questions regarding the working mechanism of plasmas on biological target. Therefore, the variable production of plasma elements has been studied, with focus on reactive species, at date considered the predominant responsible of plasma effectiveness [23]. In particular, their amounts on the target can be regulated by tuning the plasma parameters (e.g., treatment duration, distance, working gases) [2,24], achieving bivalent aims such as promoting cell proliferation and migration in would healing, or inducing cell death and apoptosis for cancer treatment and biological decontamination. Cold plasmas can be generated by a multitude of different designs, yielding differences in species output and biomedical impact [25]; [26].

One plasma source is the kINPen, an argon-driven jet which gas phase has been already well characterized. The production of primary reactive species such as excited states of argon (e.g., metastables, excimers) were observed in the effluent area (or gas phase). Those reactive species react with others gases (e.g., N_2, O_2, H_2) present in the surrounding atmosphere or in the core gas to generate secondary species, such as atomic oxygen ($\cdot O$), singlet oxygen ($^1O_2$), ozone (O_3), hydroxyl radicals (OH), superoxide anions radicals (O_2^-), hydrogen peroxide (H_2O_2), nitric oxide radicals (NO_x), acids containing nitrogen (HNO_x). Finally, a tertiary chemistry is stimulated directly in the target. Using biochemical models, covalent modification of biomolecules were predicted and observed, especially in amino acids and proteins [27–30]; and lipids [31–33].

In the cellular environment, plasma-induced biomolecules modifications could be the responsible event for the deregulation of redox signaling pathways. Indeed, it was shown that kINPen plasmas led to an abnormal production/functioning of e.g., transcription factors (e.g., Nrf2 and p53), which modulates differentially gene expressions, cellular organization and apoptosis processes [15,34–36]. Together with reactive species, radiation generated by cold plasmas could cover important synergistic effects in stimulating these processes.

In kINPen plasmas, their relevance in inducing oxidative stress must be considered, since the emission region goes from the vacuum UV region (105 nm) (emitted by argon excimers) to the near infrared (1,000 nm) [9,37]. The ultraviolet radiation (100–400 nm) emitted by kinpen plasmas could have a synergistic role in their effectiveness, e.g., for antibacterial purposes as shown also for other plasma sources [38–41].

Radiation can be generally classified in ionizing (10–125 nm), which have short wavelength, high frequency and energy, and non-ionizing (>125 nm), which oppositely are longer wavelengths with lower frequency and energy. Therefore, even if measured in low levels [42,43], vacuum UV radiation (100–200 nm) emitted by argon metastable produced by kINPen plasmas could have enough energy to impact strongly on the biological matter, leading to DNA damage, protein denaturation and cell death. Indeed, it is well known that high levels of ionizing radiation can be harmful for the living matter, generally disrupting and damaging molecular structures (e.g.,
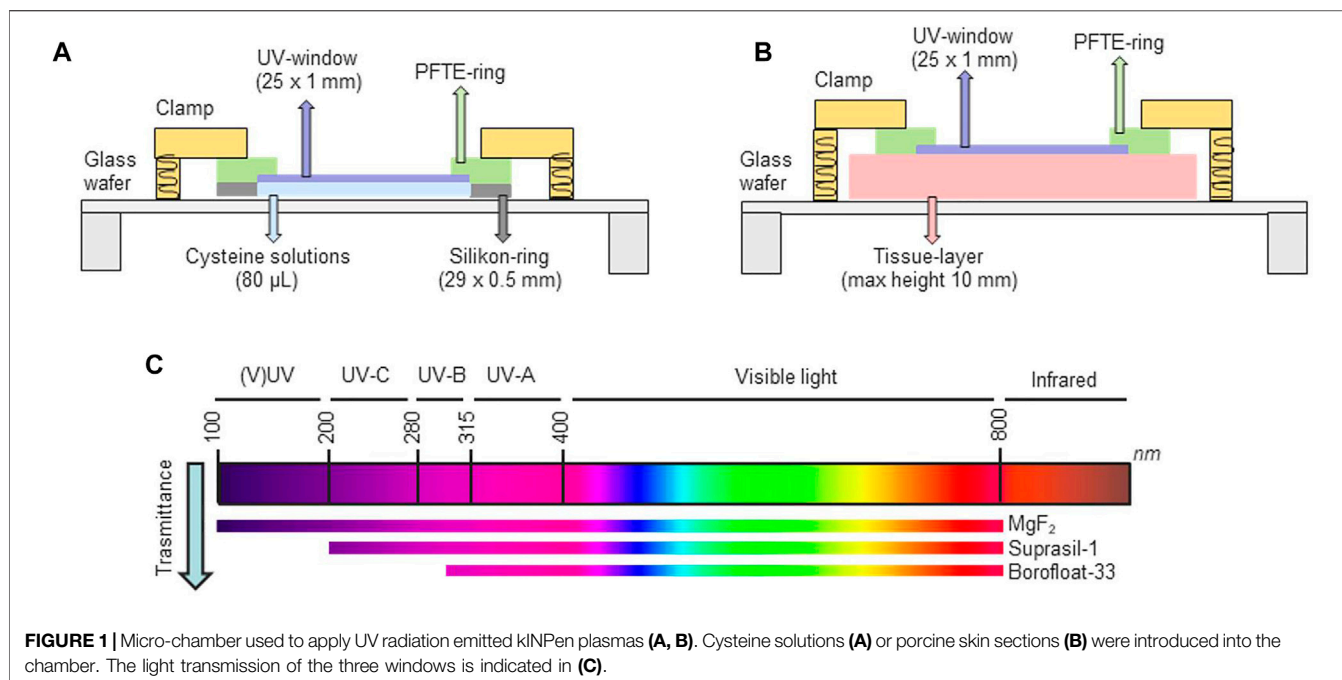
lipids, proteins, nucleic acids, carbohydrates) [44–48]. However, in relation to the quantity and time of exposure, UV radiation (mostly UV-C and UV-B, 200–315 nm) can also increase the general oxidative stress, induce indirectly or directly structural changes in biomolecules, and consequentially modulate redox signaling pathways [49,50]. The mechanism of action of radiation is still under clarification in biology, but generally they can generate biomolecules modifications by being directly absorbed (e.g., amino acids cysteine, tyrosine, tryptophan), or by stimulating sensitizing compounds (e.g., exogenous or endogenous). In both cases, excited forms will be generated, which starts photo-oxidation reactions. Indeed, radicals can be formed by hydrogen abstraction or one electron oxidation (Type I mechanism) and reactive species can be formed by energy transfer to molecular oxygen, which forms singlet oxygen (Type II mechanism) [50,51]. Generally, an increased release of reactive species from mitochondria was measured after radiation exposure, as well as the activation of a calcium dependent NOS-1 with increase of peroxynitrite levels. The chain reaction induced by photo-oxidation can be harmful in long and intense exposure, but for short and not severe exposure a transitory effect was observed, leading to a cytoprotective response mediated by MAPK1/2 activation [51]. The UV and vacuum UV light produced by different plasma sources has been considered as essential elements for the antimicrobial activity [38–41,52,53].

In this work, the role of ultraviolet radiation generated by the argon plasma jet kINPen for cysteine modifications was investigated. Cysteine is easily oxidized, and served to investigate plasma chemistry in liquids before [24,54–56]. Modifications occurring on cysteine in aqueous solutions or porcine epithelium were identified via mass spectrometry and major derivatives were quantified using it coupled to high-pressure liquid chromatography. To isolate the effects of photons from complete plasma discharge, a micro chamber equipped with VUV, UV-C, and UV-A windows was used. Alongside, optical emission spectrometry and aqueous chemistry was applied to characterize reactive species formation in the gas and liquid phase. A significant contribution of plasma derived UV radiation on cysteine chemistry was observed if water molecules were present.

2 MATERIALS AND METHODS

2.1 Sample Preparation

Crystalline cysteine (Sigma Aldrich) was solubilized in double distilled water (ddH$_2$O) to a final concentration of 2 mM on a daily basis. For short-term storage, blue ice was used to avoid pH value distortions during freeze-thawing cycles [57]. After respective plasma or irradiation treatments, solutions were immediately subjected to high-resolution mass spectrometry, multiple reaction monitoring mass spectrometry, or ion chromatography. Fresh porcine ears were received from Landmetzgerei Urich (Bad Koenig, Germany) on blue ice, serving as a well-accepted replacement model for human skin [58]. The ears were washed carefully, shaved, and the superficial

FIGURE 1 | Micro-chamber used to apply UV radiation emitted kINPen plasmas **(A, B)**. Cysteine solutions **(A)** or porcine skin sections **(B)** were introduced into the chamber. The light transmission of the three windows is indicated in **(C)**.

corneocyte layer was removed with a single CorneoFix strip (Courage and Khazaka electronic GmbH, Cologne, Germany) to increase homogenicity. Plasma treatment was performed in selected clean and homogenous areas of a 2 cm × 2 cm dimension.

2.2 Plasma Treatments

The kINPen, an argon-driven (99.999%, Air Liquide) dielectric barrier plasma jet with a flow rate of 3 standard liters per minute (slm) served as plasma source. If desired, the working gas was modified by 1% admixture of molecular oxygen (99.998, Air Liquide). Its central electrode is powered by an alternating current with a sinusoidal waveform, 2–6 kV peak–peak voltage, and a frequency of around 1 MHz. The outer electrode is insulated by a ceramic tube. The dissipated electrical power is around 1.1 W. For most experiments, a gas curtain created by a nozzle and 5 slm nitrogen (99.999%, Air Liquide) shielded the effluent from the ambient air. For details about the design and working principle of the jet, refer to Reuter and colleagues [9] and citations therein. To investigate the plasma-derived products and emitted radiation by optical emission spectroscopy, the plasma jet was positioned on axis at a distance of 9 mm to the front of a spectrometer (AvaSpec-2048; Avantes, Germany) allowing the observation of both UV and VIS/NIR range (195–980 nm) with a spectral resolution of 0.7 nm. For the VUV spectral measurements, a single grating monochromator (Acton VM-502, grating 1200 g/ mm) was used. This system was set to a spectral resolution of 0.2 nm and the spectral range of 100–200 nm was observed. Furthermore, the system was under low pressure (2.2×10^{-6} mbar) and connected via an MgF$_2$ window for VUV transmissions down to 100 nm. The kINPen was placed at 9 mm distance in front of the MgF$_2$ window.

The distance between the nozzle and the target was kept at 9 mm. Targets were either 750 μL aqueous solution in a 24 well-plate, fresh porcine skin prepared as described in 2.1, or a 25 mm diameter radiation chamber. The chamber could be equipped with windows that transmit different parts of the VUV/UV radiation and was filled with 80 μL solution forming a 500 μm thick layer or sections of porcine skin (**Figure 1A,B**). After treatments (20 s–180 s) samples were submitted to reactive species analysis (**Section 2.3**). Liquids containing the tracer molecule cysteine were also analyzed via liquid chromatography coupled to mass spectrometry for the detection of oxidative modifications (**Section 2.4**). The first 3 layers of treated porcine skin tissues were sampled using three consecutive CorneoFix strips that were immediately deposited in a protein solubilization buffer and subjected to shotgun proteomics (as described in **Section 2.5**). Each experiment was performed in triplicate.

2.3 OH and H$_2$O$_2$ Quantification via Colorimetric Assays in Liquids

For the quantification of plasma-generated, short-lived ROS (hydroxyl radicals, atomic oxygen) solution of 5 mM terephthalic acid in 25 mM phosphate buffer, pH 7.4 was used despite the limited selectivity [59]. The reaction yield to the fluorescent compound 2-hydroxyterephthalic acid (HTPA) that could be quantified at 318 nm excitation and 426 nm emission using an external calibration curve. Hydrogen peroxide deposited in treated liquids was determined using the ferrous oxidation–xylenol orange (FOX) assay according to the manufacturer's protocol (Thermo Scientific, Dreieich, Germany). The reaction yield to a purple product, which absorbance at 595 nm was

measured in a spectrophotometer (Tecan M200 multi-plate reader, Männedorf, Switzerland).

2.4 Characterization of Plasma-Induced Sulfur Chemistry in Liquids

2.4.1 Cysteine Derivatives.

Cysteine, cystine, cysteine sulfonic acid, cysteine sulfinic acid, alanine, cysteine-S-sulfonate were quantified by coupling a chromatographic separation (Agilent 1,290 Infinity II, Waldbronn, Germany) to targeted mass spectrometry (Q-Trap 5500, Sciex, Darmstadt, Germany). Analytes were separated on a 2.1 mm × 100 mm Acquity Amide Column with 130 Å pore size and 1.7 μm particle size and a corresponding VanGuard precolumn (Waters, Manchester, England) at a column temperature of 35°C. Mobile phase A consisted of 10 mM ammonium formate in water plus 0.15% formic acid while B consisted of 10 mM ammonium formate in acetonitrile plus 0.15% formic acid. The flow rate was 0.8 ml/min. A linear gradient was applied (0.0 min–99% B; 4.0 min–85% B; 7.0 min–30% B; 7.1 min–99% B; 9.0 min–99% B). Prior to injection, samples were diluted 1:5 in mobile phase B. Compounds were determined via multiple reaction monitoring in positive mode. The electrospray (ESI) source parameters were the following: curtain gas 35 psi, gas 1 20 psi, gas 2 25 psi, temperature 150°C, 5.5 kV probe voltage, 50 V declustering potential. The transitions and the correspondent collisional energies (CE) used for each compounds were for cysteine $122 \rightarrow 76$ m/z, CE 20; cystine $241 \rightarrow 152$ m/z, CE 10; cysteine sulfinic acid $154 \rightarrow 74$ m/z, CE 20; cysteine sulfonic acid $170 \rightarrow 124$ m/z, CE 10; cysteine-S-sulfonate $202 \rightarrow 120$ m/z, CE 10; alanine $90.1 \rightarrow 44.1$ m/z, CE 8. External calibration curves allowed the absolute quantification of the listed compounds in plasma-treated or irradiated samples.

2.4.2 Hydrogen Sulfide.

To quantify the formation of hydrogen sulfide (H_2S) from cysteine, the monobromobimane (mBB) assay was optimized [60]. A solution of 100 mM MBB in acetonitrile was freshly prepared. First, 25 μL of analyte solutions was mixed with 2 μL MBB and 65 μL of 100 mM phosphate buffer at pH 7.8. After vigorous mixing, samples were incubated at 37°C for 10, 30, or 60 min using a thermomixer, yielding sulfodibimane (SDB) in the presence of H_2S. The reaction was stopped by adding 5 μL formic acid 50% and cleared by centrifugation. SDB was quantified by targeted mass spectrometry. Analytes were separated on a 2.1 × 50 mm Zorbax RRHD Eclipse Plus C18 column (Waters, 95 Å pore size, 1.8 μm particle size) and corresponding guard column. Mobile phases were water (A; Th. Geyer, Renningen, Germany) and acetonitrile (B; ibid). A linear gradient was applied (0 min–5% B; 2.1 min–40% B; 5 min–40% B; 5.1 min–98% B; 6 min–98% B; 6.1 min–5% B; 8 min–5% B). The flow rate was of 0.8 ml/min. Atmospheric pressure chemical ionization (APCI) was applied with the following source parameters: curtain gas 20 psi, gas 1 50 psi, temperature 500°C, 3 kV needle current, 100 V declustering potential, 32 V collision energy. The transitions used

for the analyzed compounds were for MBB $272 \rightarrow 193$ m/z; SDB $415.1 \rightarrow 193.3$ m/z.

2.4.3 Sulfite and Sulfate.

Ion chromatography (ICS-5000, Dionex Corp., Sunnyvale, United States) was used for the quantification of sulfite (SO_3^-) and sulfate (SO_4^-) anions. These were separated on a IonPac® AS23 pre-column (2 × 50 mm) coupled to an IonPac® AS23 anion exchange column (2 × 250 mm, Thermo Fisher Scientific Inc., Waltham, United States). Isocratic separation was achieved using a carbonate buffer (4.5 mM Na_2CO_3/0.8 mM $NaHCO_3$) and the flow rate of 0.25 ml/ min.

2.5 Investigation of Protein Modifications in Tissues

2.5.1 Protein sample preparation.

After sampling via tape stripping controls and plasma treated porcine skin layers, proteins were solubilized by introducing the tape strip in 500 μL of SDS-based lysis buffer (5% SDS, 50 mM TEAB pH 7.55) and by vortexing the vials for 2 min at room temperature. A S-Trap midi spin column digestion protocol from ProtiFi was applied according to the manufacturers protocol. The solutions were sonicated to disrupt cells, dissolve proteins, and shear DNA and clarified by centrifugation at 4000g for 10 min at 4°C. The supernatant was transferred to a clean vial. The reduction and alkylation of sulfhydryl groups was performed by incubating respectively with 5 mM tris(2-carboxyethyl) phosphine (TCEP, 55°C, 15 min) and subsequently with 20 mM methyl methanethiosulfonate (MMTS) at RT for 10 min. The reaction was stopped by adding 12% phosphoric acid. Next, 300 μL S-Trap buffer (90% methanol, 100 mM TEAB, pH 7.1) was added, and samples were transferred to the spin column. After centrifugation (2 min × 4000 g), the column was washed with 300 μL S-Trap buffer three times. Protein digestion was achieved in column by adding 1:25 wt:wt sequencing grade trypsin (Promega, Madison, United States) in 50 mM TEAB and incubating for 1 hour at 47°C. In this case, the columns were sealed with a lid to avoid solution evaporation. Finally, peptides were eluted with 500 μL of acetonitrile containing 0.2% formic acid. The solutions were dried using a SpeedVac and resuspended in 10 μL of water containing 0.1% formic acid before nanoLC-MS analysis.

2.5.2 LC-MS analysis.

The proteomes and the oxidative modifications occurring in porcine skin layers after treatments were analyzed by nanoflow liquid chromatography, using an UltiMate 300 RSLCnano coupled to a QExactive Hybrid-Quadrupol-Orbitrap from Thermo Fisher Scientific, Dreieich/Germany. The technical details of the separation and detection are described in Wenske et al., 2021. Raw data were analyzed with the Proteome Discoverer 2.4 (Thermo Fischer Scientific) and the Byonic 3.6.0 node (Protein Metrics) for searching protein modifications. A list of 15 modifications previously identified for gas plasma treatments of thiol moieties was used to reduce

TABLE 1 | Analyzed thiols oxidative modifications occurring in the proteome of plasma treated porcine skin samples.

Mass shift (Da)	Composition	Modification	Acronym	Label
−2.02	−2H	Dehydrogenation	Didehydro	A
+15.99	+O	Oxidation	Oxidation	B_1
+21.98	+2O	Dioxidation	Dioxidation	B_2
+47.98	+3O	Trioxidation	Trioxidation	B_3
+28.99	+N + O -H	Nitrosylation	Nitrosyl	C1
+44.98	+N +2O -H	Nitration	Nitro + O	C2
−15.01	−N −H	Deamination	−NH	D_1
−17.03	−N −3H	Deamination + Dehydrogenation	−NH3	D_2
−31.97	−S	Sulphur loss	−S (alanine)	E_1
+31.97	+S	Sulphur addition	+S	E_2
+79.96	+S +3O	Sulfonylation	+SO3	E_3
+119.00	+S +3C +5H + N +2O	Cysteine addition	+S2R	F_1
+150.99	+S +3C +5H + N +4O	Cysteine addition + Dioxidation	+S2O4R	F_2
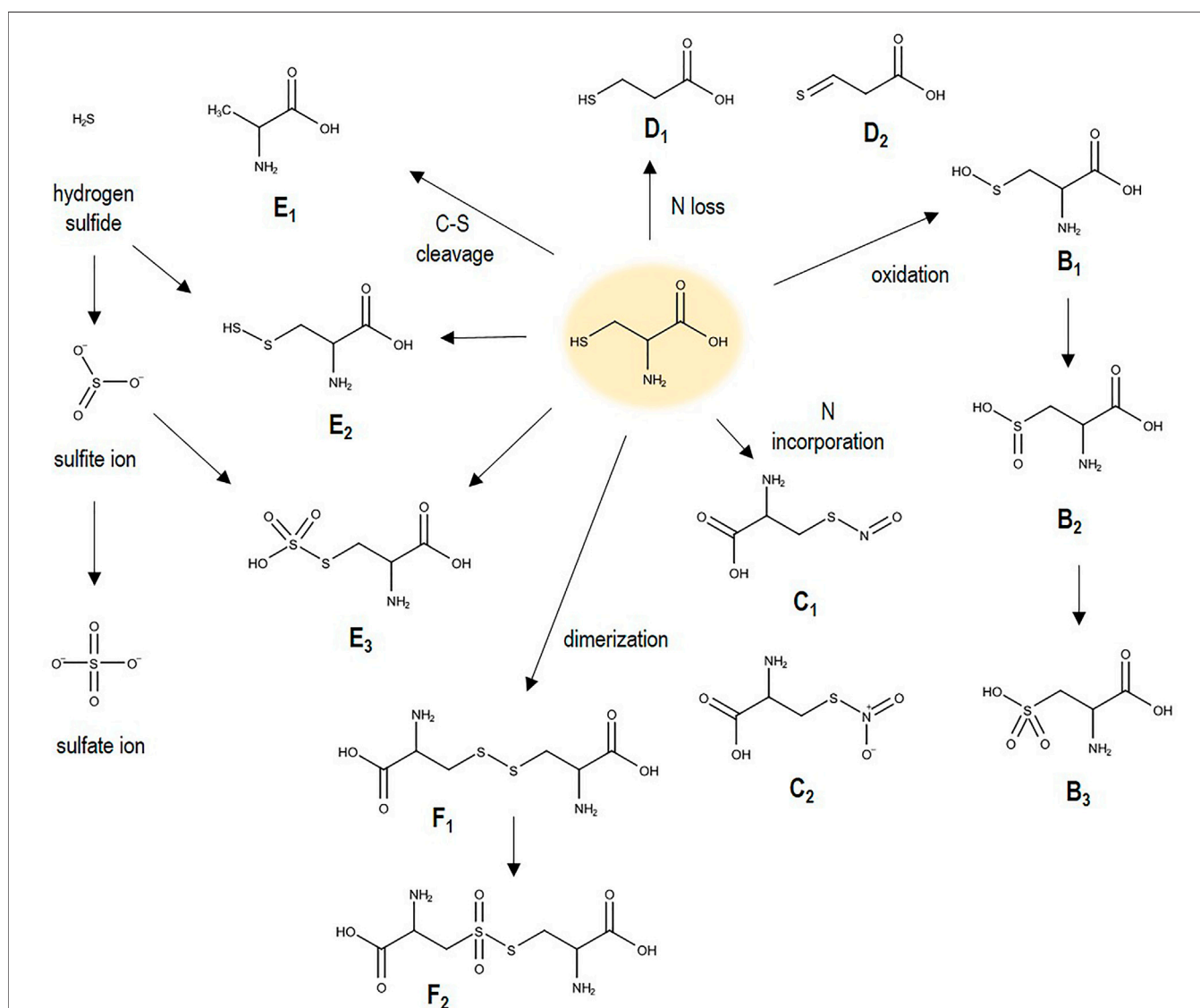
FIGURE 2 | Cysteine oxidation and cleavage products (see **Tables 1**, **2**). When incorporated into a protein, the carboxyl and amino group are incorporated in the peptide bond.

FIGURE 3 | OES spectra registered at 9 mm distance from jet nozzle in the range 195–465 nm (UV range, **(A and C)** and 430–980 nm (VIS/NIR range, **(B and D)**. **(A and B)**: kINPen09, 3 slm Ar, **(C and D)**: kINPen09/3slm Ar + 0.5% oxygen. Free plasma jet, and radiation filtered through MgF₂ (transparent >125 nm), Suprasil (quartz based, > 195 nm), and Borofloat glass (>300 nm) were compared (see legend in spectra). Due to limitations in setup (no measurements <195 nm), only slight changes between 200 and 300 nm were observed. The VIS/NIR region remained unchanged by the different windows except for a minor reduction in intensity.

calculation times (**Table 1**) [24,55]. A maximum of three modifications per peptide was set, and to ensure result validity, only peptides with a Byonic score >250 and a Delta Mod score of >5 were accepted for downstream data analysis. A normalization on the total peptides containing cysteine was performed, yielding a percentage of modified thiols on the total proteome. Furthermore, the oxidative modifications found in controls were subtracted as background from all other samples and data are shown as difference from the control. One-way ANOVA statistical test was performed in order to detect significant modifications, allowing a comparison between different conditions.
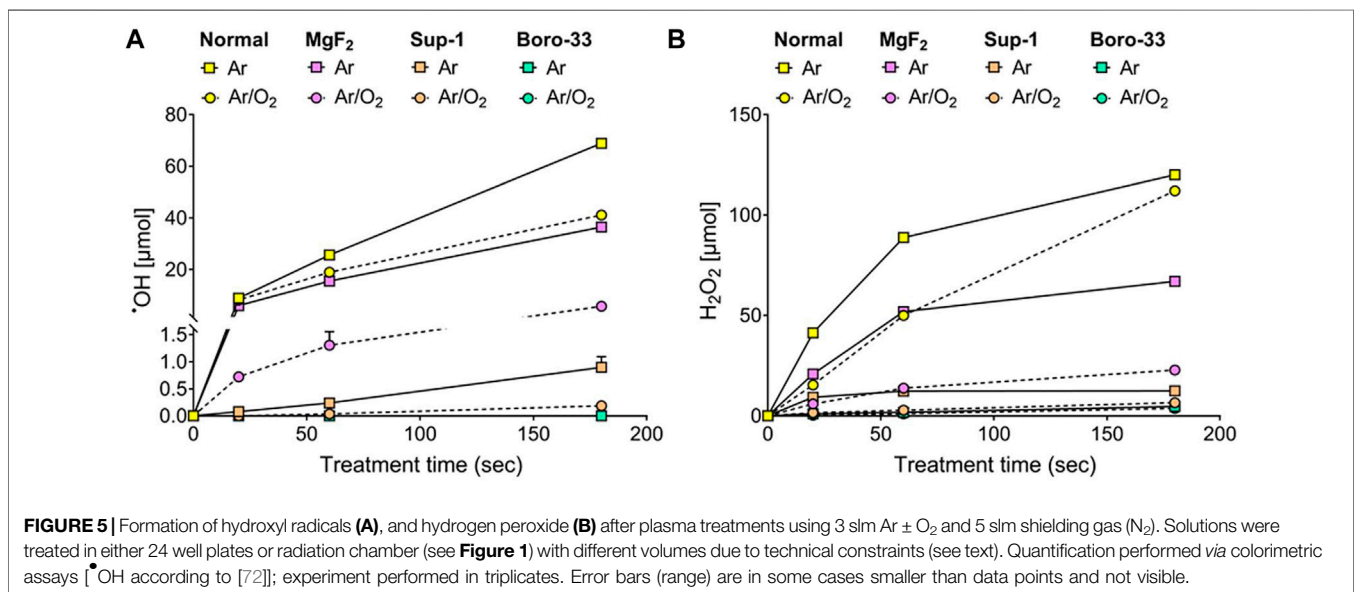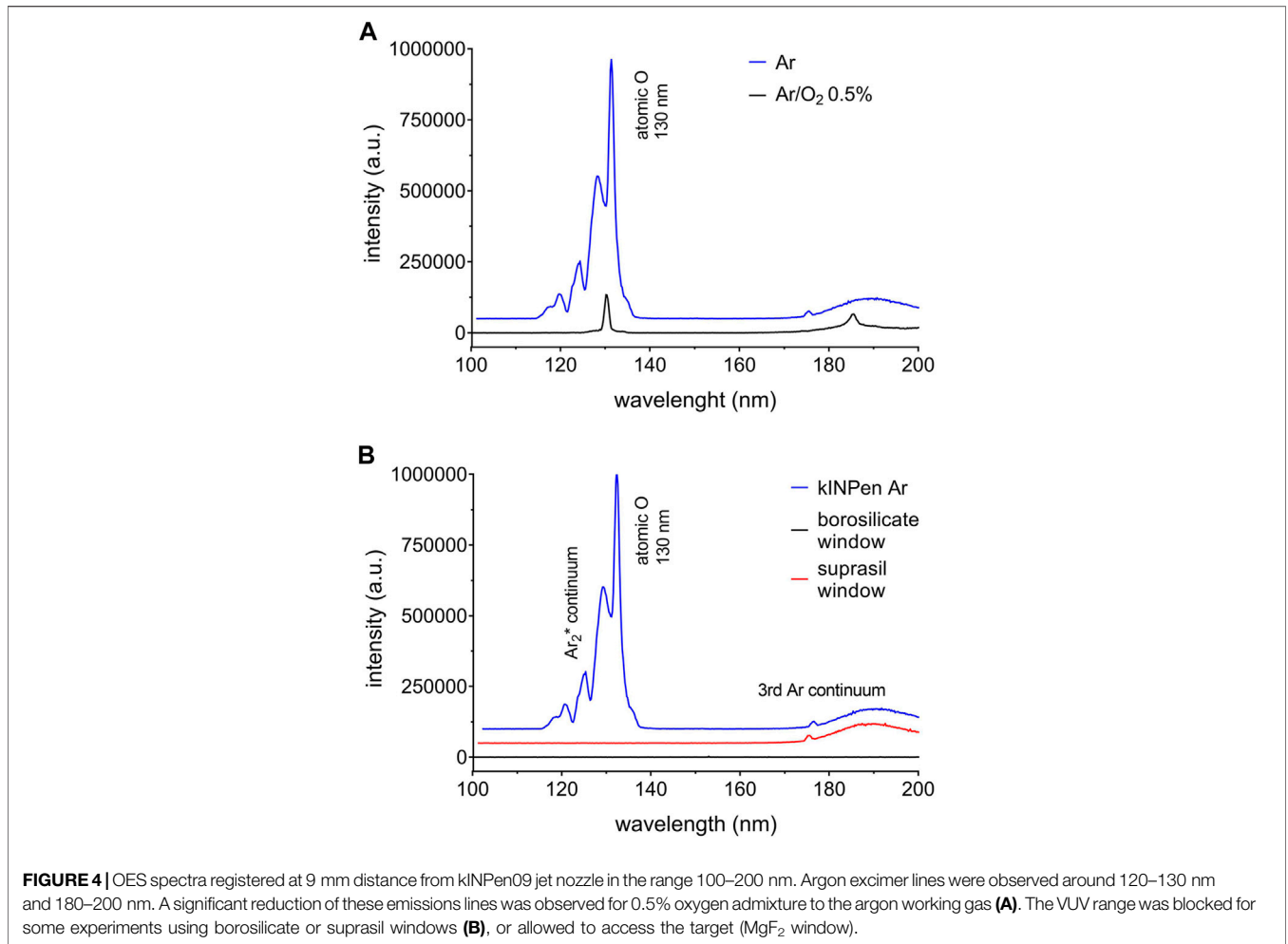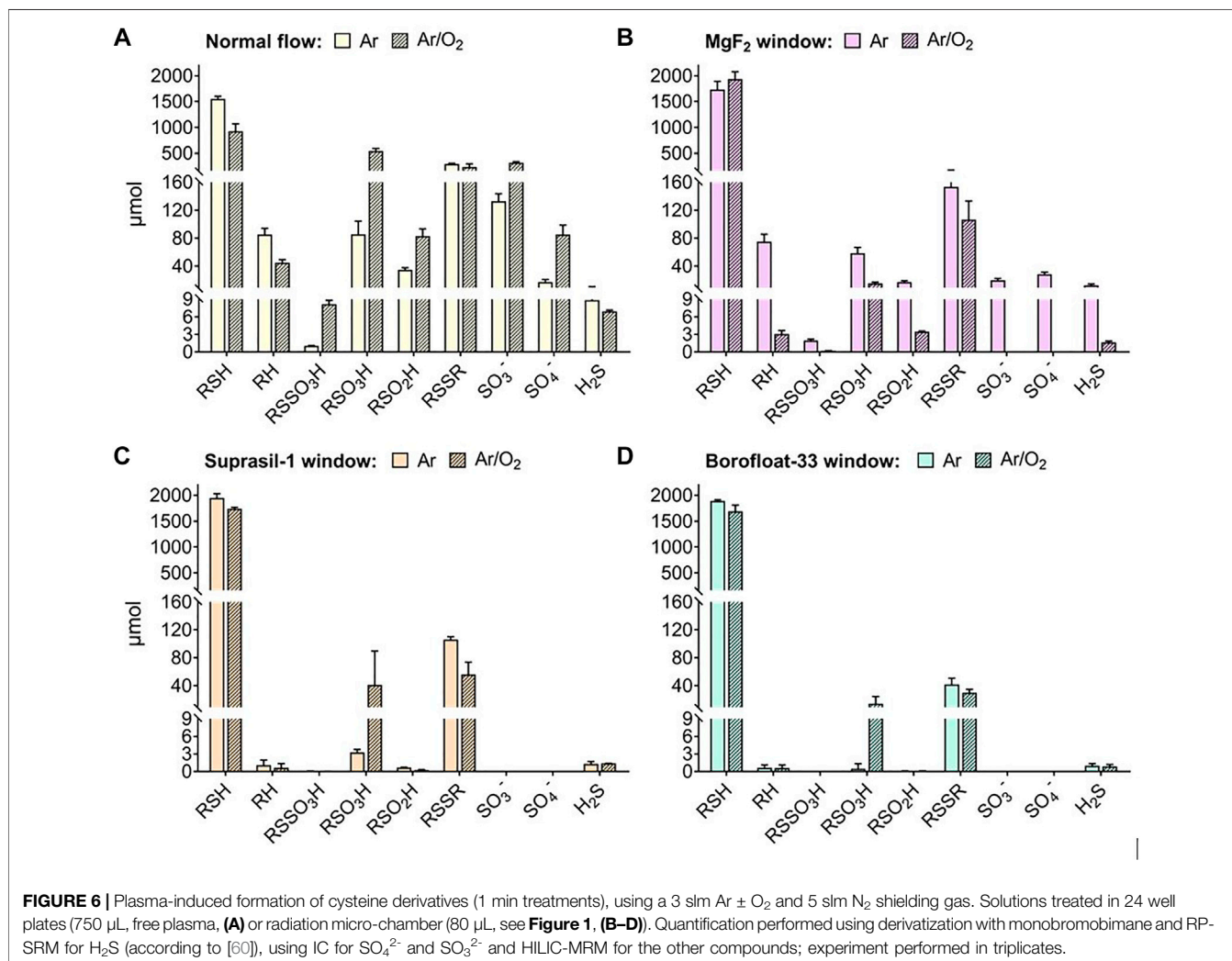
FIGURE 4 | OES spectra registered at 9 mm distance from kINPen09 jet nozzle in the range 100–200 nm. Argon excimer lines were observed around 120–130 nm and 180–200 nm. A significant reduction of these emissions lines was observed for 0.5% oxygen admixture to the argon working gas **(A)**. The VUV range was blocked for some experiments using borosilicate or suprasil windows **(B)**, or allowed to access the target (MgF$_2$ window).

FIGURE 5 | Formation of hydroxyl radicals **(A)**, and hydrogen peroxide **(B)** after plasma treatments using 3 slm Ar ± O$_2$ and 5 slm shielding gas (N$_2$). Solutions were treated in either 24 well plates or radiation chamber (see **Figure 1**) with different volumes due to technical constraints (see text). Quantification performed *via* colorimetric assays [•OH according to [72]]; experiment performed in triplicates. Error bars (range) are in some cases smaller than data points and not visible.

TABLE 2 | Analyzed cysteine derivatives, acronyms, formulas, quantification method and responsible plasma element.

Name	Acronym	Hill notation	Analysis	Plasma element
Cysteine	RSH	$C_3H_6NO_2S$	HILIC-MRM	None
Cystine	RSSR	$C_6H_{12}N_2O_4S_2$	HILIC-MRM	Radicals
Alanine	RH	$C_3H_7NO_2$	HILIC-MRM	(V)UV
Sulfonic acid	RSO_3H	$C_3H_7NO_5S$	HILIC-MRM	$\dot{O}H$, $^1O_2$, $\dot{O}$
Sulfinic acid	RSO_2H	$C_3H_7NO_4S$	HILIC-MRM	$\dot{O}H$, $^1O_2$, $\dot{O}$
S-sulfonate	$RSSO_3H$	$C_3H_7NO_5S_2$	HILIC-MRM	$\dot{O}H$, $\dot{O}$ (indirect)
Sulfite	SO_3^-	O_3S	IC	(V)UV, $\dot{O}H$, $^1O_2$, $\dot{O}$
Sulfate	SO_4^-	O_4S	IC	(V)UV, $\dot{O}H$, $^1O_2$, $\dot{O}$
Hydrogen sulfide	H_2S	H_2S	MBB, RP-MRM	(V)UV

FIGURE 6 | Plasma-induced formation of cysteine derivatives (1 min treatments), using a 3 slm Ar ± O₂ and 5 slm N₂ shielding gas. Solutions treated in 24 well plates (750 μL, free plasma, **(A)** or radiation micro-chamber (80 μL, see **Figure 1**, **(B–D)**). Quantification performed using derivatization with monobromobimane and RP-SRM for H₂S (according to [60]), using IC for SO_4^{2-} and SO_3^{2-} and HILIC-MRM for the other compounds; experiment performed in triplicates.

3 RESULTS AND DISCUSSION

3.1 Fingerprinting the kINPen Plasma Radiation

The kINPen spectra of emission goes from the vacuum UV (100 nm) to the near infrared (1,000 nm) [61]. The intensity of the UV irradiation was determined to be around 100 μJ cm⁻².

Optical emission spectroscopy was performed in order to characterize the emission spectra of the applied plasma treatment conditions (**Figure 1**). In this case, the emission spectra were measured applying the three different windows filtering various radiation ranges (**Figure 2**). Additionally, the vacuum UV range was recorded using a vacuum setup (**Figure 3**) [9,37]. In pure argon, emission lines from impurities of •OH and

N_2 were measured between 300 and 350 nm, and small atomic oxygen lines at 777 and 844 nm. The infrared region was dominated by argon emission lines, while between the range 400–700 nm no emission was observed. In the vacuum UV region (<195 nm), a dominant continuum centered at 126 nm can be measured for argon excimer (Ar_2^*), which includes also small absorption lines from ozone and O_2. The modulation of working or shielding gases, induced changes in the emission spectra, e.g., the addition of molecular oxygen in the working gas leads to a reduction of Ar_2^* emission lines and increase those oxygen-based [9,37]; (Figure 2). The presence of molecular O_2 in the working gas interfered with the gas phase chemistry and UV emission of various species, such as $^\bullet$OH, N, $^\bullet$NO, and Ar_2^*. Suprasil and Borofloat-33 scavenged the emission of argon excimers, while in the range between 195 and 465 more subtle changes were observed, reflecting the characteristics of normal glass (Figure 2). Particularly in conditions with pure argon, which are certified for medical applications with kINPen MED, the role of vacuum UV radiation was dominant (Figure 3). As discussed previously, this event could be due to the lower formation of gaseous reactive species and therefore less reactions of argon metastable and excimers with surrounding gases to form further species, e.g., ozone, atomic oxygen, singlet oxygen, etc. [9,37]; (Figures 2, 4).

3.2 Vacuum UV as Source of Water-Derived $^\bullet$OH and H_2O_2 Production

The formation of $^\bullet$OH and H_2O_2 in water was compared using full plasma treatments (3 slm Ar and Ar + 1% O_2) and treatments using windows filtering different radiation ranges (Figure 5). The dissociation of water yielding OH radicals was favored in full argon plasma treatments and when VUV radiation was admitted (MgF_2-window). For short treatments only small differences in $^\bullet$OH production was observed, but enlarging with treatment time. Full argon plasma produced around 30 µmol of $^\bullet$OH more than Ar plasma/MgF_2-window. It may be argued that either OH radicals from the gas phase contributed here or atomic oxygen generated from impurities. A recent report showed the sensitivity of terephatalic acid to this reactive short-lived species. Also liquid dynamic effects increasing the contact area between emitted radiation and target in contrast to the static treatments performed in the micro-chamber can contribute. Upon addition of molecular oxygen to the working gas, a decrease in $^\bullet$OH and H_2O_2 production was observed, especially when the MgF_2-window was used, blocking interphase chemistry. In the near-complete absence of VUV radiation from the argon excimers, water dissociation did not occur. Corroborating this observation, almost no OH/H_2O_2 formation was sparked by the longer UV ranges (UV-C and B and UV-A, respectively Suprasil-1 and Borofloat 33). Therefore, oxygen-base emission lines (atomic oxygen in NIR, ozone and O_2 in VUV), which increases in presence of molecular oxygen in the working gas, did not led to water dissociation. However, their potential direct impact on cysteine structures was investigated [55]. Overall, being highly energetic, VUV radiation emitted by Ar_2^* were able to induce water ionization, in contrast to the other UV ranges.

Therefore, the direct and indirect (e.g., water-derived species production) impact of VUV radiation resulted as predominant responsible of the effects induced on the liquid target. In the presence of oxygen in the gas phase, species derived from interphase chemistry and/or chemistry in liquid bulk are dominant, while VUV radiation is eliminated (Figure 3A).
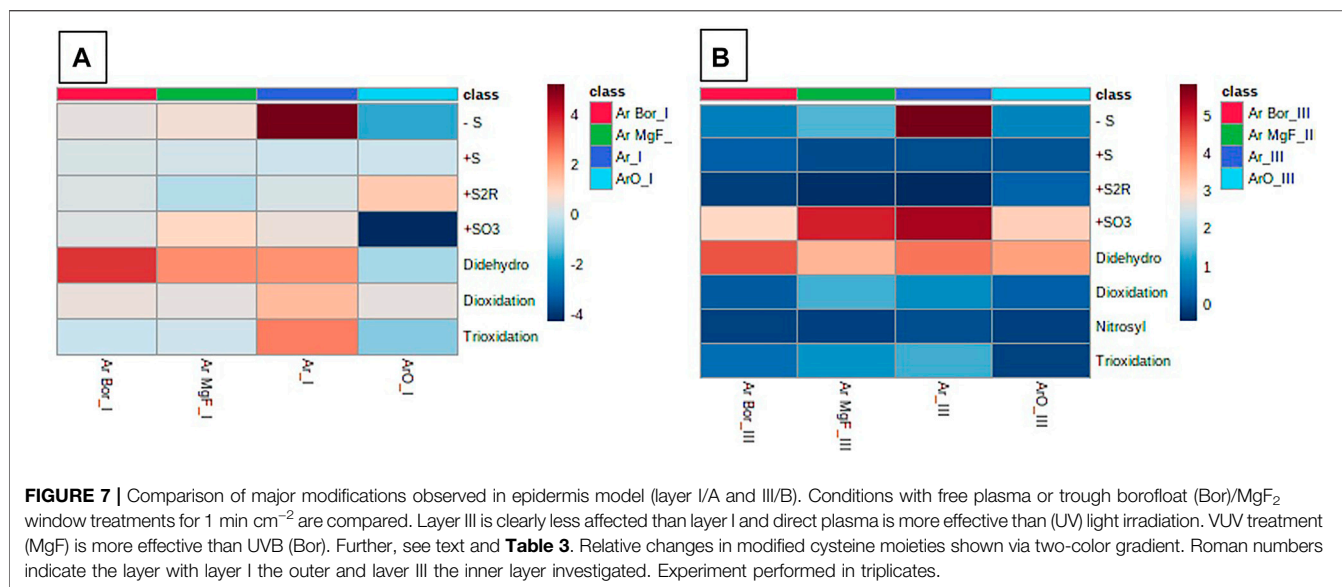
3.2 Direct and Liquid-Mediated Effects of Radiation on Cysteine Solutions

The impact of full plasma treatments and plasma-generated UV/VIS/NIR light on cysteine molecules is shown in Figure 6. Table 2 shows the structures, the quantification methods, and the major plasma components involved in the generation of each cysteine derivative. As discussed, argon plasma conditions stimulated predominantly pathways in liquid via impact of VUV radiation emitted by argon excimers, leading to $^\bullet$OH and H_2O_2 production. The same experiments were performed with cysteine containing solutions. The formation of products that derive from the loss of the thiol group in cysteine (alanine, cysteine-S-sulfonate, sulfite ions, sulfate ions, and hydrogen sulfide) was almost identical in treatments with full argon plasmas and filtered VUV radiation of argon plasmas (MgF_2). In contrast, these products almost disappeared when VUV-impermeable oxygen was introduced to the working gas and gas–liquid phase chemistry was blocked by an MgF_2-window. This confirmed the key role of VUV radiation, leading to a cleavage of the carbon-sulfur bond [63], that was not observed by using other windows/radiation ranges. The energy of this bond is 272 kJ mol^{-1}, weaker than other bonds in cysteine or water (H-O 465 kJ mol^{-1}, C-C 347 kJ mol^{-1}, S-H 347 kJ mol^{-1}). The energy of the impinging UV photons of the argon excimer lines is much higher, 949 kJ mol^{-1} (126 nm), allowing the cleavage of all bonds present in the target, including the oxygen-hydrogen bond in water molecules. Accordingly, it might be argued that OH radical formation is the first step ultimately yielding in thiol moiety abstraction. However, the presence of hydrogen sulfide (H_2S) clearly indicates that a direct cleavage of the C-S bond contributes significantly or is even dominant considering the weaker bond energy compared to the H-O bond. Interestingly, no indications of a C-C bond breakage in cysteine, leading e.g. to the formation formic acid, was observed. Summarizing, conditions with pure argon showed a significant contribution of the VUV radiation, stimulating i) the production of OH radicals, and ii) C-S bond breakages. Under VUV radiation, derivatives such as cystine and cysteine acids were also produced in consistent amounts in relation to full argon plasmas. The origin of the oxygen incorporated in structures such as sulfite, sulfate, cysteine acids and S-sulfonate, in this case, are water-derived species [55].

As previously discussed, due to the controlled pH (7.2), only low amounts of thiolate were available to react with H_2O_2 since the pKa of the cysteine thiol group is 8.18—allowing less than 5% deprotonation. Therefore, a minimal role in thiol oxidation could be attributed to hydrogen peroxide. Furthermore, a two-step reaction would be needed to form cystine: a first reaction of H_2O_2 with thiolate, with formation of cysteine sulfenic acid, and a second reaction of RSOH with another thiolate [63]; [64]. More

TABLE 3 | Cysteine focused protein modifications observed in porcine epidermis model (ANOVA and Post-hoc analysis Fisher's LSD, p-value and FDR ≤0.05).

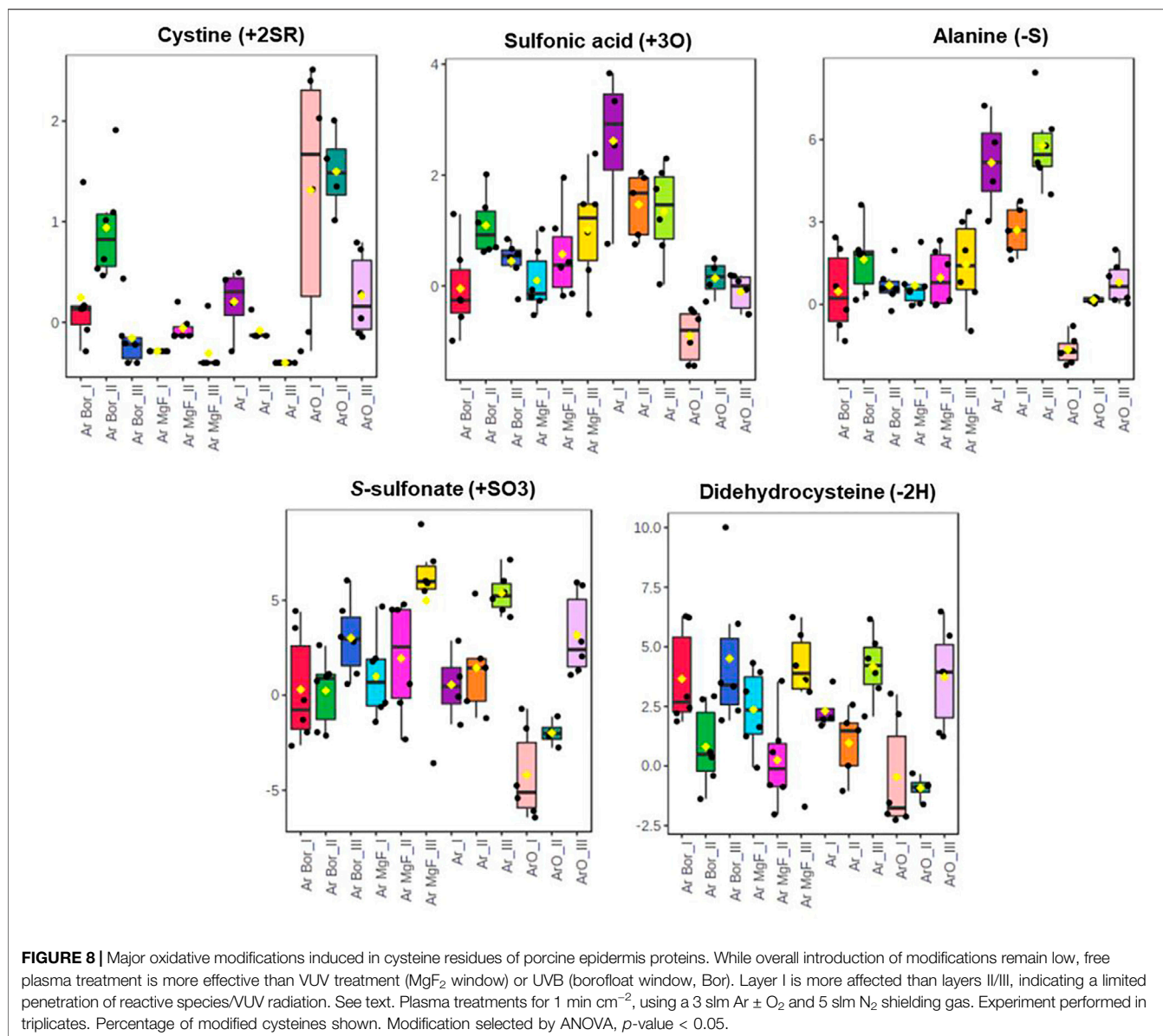|	$p < 0.05$ (n)	Type of modification
Overall	5	sulphur loss (-S), Trioxidation, Sulfonylation (+SO3), Cysteine addition (+S2R), Didehydrogenation (didehydro)
Layer I	5	Sulphur loss (-S), Trioxidation, Sulfonylation (+SO3), Cysteine addition (+2SR), Didehydrogenation (didehydro)
Layer II	3	Cysteine addition (+S2R), Nitrosylation (nitrosyl), Sulphur loss (-S)
Layer III	3	Sulphur loss (-S), Cysteine addition (+S2R), Trioxidation
Ar/O2 plasma	5	Nitrosylation (nitrosyl), Sulphur loss (-S), Sulfonylation (+SO3), Trioxidation, Didehydrogenation (didehydro)
Ar plasma	4	Cysteine addition (+S2R), Sulfonylation (+SO3), Didehydrogenation (didehydro), Sulphur loss (-S)
Ar MgF2 window	1	Nitrosylation (nitrosyl)
Ar Borofloat window	1	Cysteine addition (+S2R)

FIGURE 7 | Comparison of major modifications observed in epidermis model (layer I/A and III/B). Conditions with free plasma or trough borofloat (Bor)/MgF$_2$ window treatments for 1 min cm^{-2} are compared. Layer III is clearly less affected than layer I and direct plasma is more effective than (UV) light irradiation. VUV treatment (MgF) is more effective than UVB (Bor). Further, see text and **Table 3**. Relative changes in modified cysteine moieties shown via two-color gradient. Roman numbers indicate the layer with layer I the outer and layer III the inner layer investigated. Experiment performed in triplicates.

likely, the reaction of $^\bullet$OH with cysteine generates cystine by first formation of thiyl radicals (RS$^\bullet$), which rapidly recombine to form cystine. The formation of cysteinyl radicals was detected using BMPO/EPR spectroscopy earlier [54].

The reaction of RS$^\bullet$ with $^\bullet$OH would lead to cysteine sulfenic acid, which immediately is oxidized into sulfinic and further to sulfonic acid by $^\bullet$OH or H$_2$O$_2$ [65–67]. The production of S-sulfonate (RSSO$_3$H), in absence of atomic oxygen, could be promoted by first cystine oxidation by two $^\bullet$OH, with following C-S breakage promoted by VUV and final incorporation of another oxygen. Sulfite can be generated by cut of the C-S bond in cysteine sulfonic acids, or most likely, cysteine S-sulfonate (S-S bond dissociation energy 414.6 kJ mol^{-1}) [68]. Supplementary experiments have been performed by treating cysteine sulfonic acid in the radiation chamber, as shown in the supplementary material (**Supplementary Figure S1**). Despite the high concentration of the reference compound cysteine sulfonic acid, only small amounts of sulfite and sulfate ions are formed, indicating that the majority of C-S bond cleavages takes place at the cysteine or cystine level. With that, most sulfite and sulfate ions were generated by the oxidation of H$_2$S. This pathway is favored in the presence of reactive oxygen species produced by the cleavage water molecules (e.g. H$_2$O$_2$, $^\bullet$OH). Clearly, a number

of chemical pathways were active in liquids under the influence of vacuum UV radiation, in contrast to radiation >195 nm (UV-C).

The cysteine products generated by UV-C (Suprasil) or UVB/UVA (Borofloat) were clearly different. In these cases, almost no production of the water-derived species OH/H$_2$O$_2$ (**Figure 5**) and cysteine derivatives generated by C-S bond cleavage (SO$_4$$^{2-}$, SO$_3$$^{2-}$, alanine/RH; **Figure 6**) were observed.

The formation of cystine via hydrogen abstraction in cysteine (type I photo-oxidation mechanisms) and RS$^\bullet$ recombination [50,51]; was observed independent from the window, but with lower extent when vacuum UV is blocked (Borofloat/Suprasil). The production of sulfonic acid (RSO$_3$H, **Figure 6**) was measured in conditions with oxygen in the working gas, suggesting the potential role of radiation emitted in the near infrared and depending by the presence of O$_2$. The origin of oxygen incorporated by sulfonic acid, in this case, could be due to the reaction of thiyl radical with water, generating $^\bullet$OH by hydrogen abstraction. Even though the radiation emitted in these ranges are not ionizing, due to the lower energy, it was shown that also the UV radiation >200 nm can induce oxidative stress in cellular compartments in relation to the exposure time, with increase in the cellular production of reactive species [49,50].

FIGURE 8 | Major oxidative modifications induced in cysteine residues of porcine epidermis proteins. While overall introduction of modifications remain low, free plasma treatment is more effective than VUV treatment (MgF_2 window) or UVB (borofloat window, Bor). Layer I is more affected than layers II/III, indicating a limited penetration of reactive species/VUV radiation. See text. Plasma treatments for 1 min cm^{-2}, using a 3 slm Ar $\pm$ O$_2$ and 5 slm N$_2$ shielding gas. Experiment performed in triplicates. Percentage of modified cysteines shown. Modification selected by ANOVA, p-value < 0.05.

3.3 Plasma Radiation Impact on Epidermal Protein Structures

The analysis of the oxidative modifications of cysteine belonging to the porcine epidermal proteome was performed via tape stripping assay in combination with high-resolution mass spectrometry. The oxidation was monitored in the first three stratum corneum layers of the porcine epidermis, reflecting a penetration depth of 5–7 µm. **Table 3** and **Figure 7** give an overview of the detected modifications, while **Figure 8** shows a quantitative comparison of the most relevant oxidative modifications. Unstable oxidative modifications, such as S-nitrosylation, may have been underestimated. According to proteomics standard procedures, thiols were reduced and alkylated during sample workup. Some losses to the plasma chemistry on protein thiols (e.g., sulfenic acids,

S-nitrosylation) cannot be excluded although stable modifications (e.g., cysteine sulfonic acid, cysteine-S-sulfonate) were retained. Overall, five types of modifications were found to be introduced into the epidermal proteins with a statistical significance. These are the apparent replacement of cysteine by alanine (sulphur loss), the formation of cysteine sulfonic acid (trioxidation), the formation of cysteine-S-sulfonate (sulfonylation), the formation of a disulfide with other cysteine moieties (+S2R), and the loss of two hydrogen atoms forming an unsaturated cysteine molecule (didehydrogenation) (**Table 3**). Alongside depth in the epidermis, the intensity and number of detected modifications decrease (**Figure 7**). The impact of plasma-derived UV or VUV light was lower than expected from the *in vitro* experiments (**Table 3**). Only nitrosylation was found to be significantly elevated by MgF_2 filtered kINPen irradiation, pointing at a limited role of (V)UV photons *in vivo*.

The conversion of cysteine in cysteine S-sulfonate (+SO_3) and dehydrogenated cysteine (-2H) (**Figure 8**), was promoted especially in the third skin epidermis layer, regardless of the applied treatment condition. The results indicate that protein modifications result from complex dynamics and are not corresponding to the action of only one plasma components produced in specific conditions.

Some modifications appear in special conditions only. For example, the conversion of cysteine into cystine was observed in treatment with Ar/O_2 full plasmas, with a maximum in the first layer and a progressive decrease in the second and third. In this condition, the effluent contains significant amounts of singlet oxygen and atomic oxygen, especially at short distances from the nozzle. Atomic oxygen is able to form thyil radicals by hydrogen abstraction to the protein cysteines, which rapidly may recombine forming a disulfide bond. This event causes conformational changes of the protein, alongside a potential gain or loss of function. The oxidation of cysteine into sulfonic acid by the incorporation of three oxygen atoms, and the breakage of the C-S bond with conversion of cysteine to alanine were events observed predominantly in treatments with full argon plasma in the first layer of the skin. When using windows, even in case of the VUV-transmitting MgF_2 and more prominent in suprasil and Borofloat-33 windows, only few such modifications were detected. This indicates that the VUV radiation, although most prominent in Ar plasma, does in soft targets not contribute in the same manner to biomolecule modification than in liquid targets. In this case, the direct impact of argon metastables and other gas phase species and the subsequent formation of secondary reactive species is more prominent. This is in line with a report investigating the oxidation of human skin lipids that showed a limited impact of the argon plasma on lipid side chain oxidation in the absence of water [33]. Obviously, the highly energetic VUV radiation is unable to penetrate deeper into layers of biomolecules such as the model described here or the sebum lipids, limiting its ability to contribute significantly to the plasma chemistry *in situ*.

4 CONCLUSION

In aqueous targets (**Sections 3.2, 3.3**), plasma-derived VUV radiation is an effective component in plasma-liquid chemistry. The liquid phase acts as compartment amplifying the plasma chemistry by the *de novo* formation of secondary water-derived reactive species (e.g., hydroxyl radicals, hydrogen peroxide) at the gas-liquid interphase, that subsequently allow the modification of sensitive targets such as thiol moieties. In contrast, in complex targets like the intact skin the plasma-derived VUV radiation is blocked effectively by the dense biomolecules layers and plays a limited role only. While this might be disappointing from the scientific

viewpoint it emphasizes the safety of physical plasmas which has been a significant concern for years. Corroborating a number of reports proofing the safety [69]; [70]; [71], our results further support the safe application of physical plasmas. Even in humid wounds where resident water molecules allow the formation of secondary species by the UV radiation increasing the effectiveness of plasma while the protein layer in the wound bed protects the local tissue.

Proteomics Data
The proteomics data connected to this paper have been uploaded to the ProteomeXchange servers under the project name "Gas plasma and (V)UV impact on porcine epidermis using a tape strip assay approach" (Project accession: PXD028915, username: reviewer_pxd028915@ebi.ac.uk/Password: OPKS8hii).

DATA AVAILABILITY STATEMENT

The datasets presented in this study can be found in online repositories. The names of the repository/repositories and accession number(s) can be found below: ProteomeXchange with accession PXD028915.

AUTHOR CONTRIBUTIONS

GB, KW, and TvW devised the experiments, wrote an corrected the manuscript HM and TG performed OES measurements and discussed the data GB, SW, and KW performed mass spectrometry analysis and discussed the data/incorporated it into the manuscript.

FUNDING

ACKNOWLEDGMENTS

SUPPLEMENTARY MATERIAL

The Supplementary Material for this article can be found online at: https://www.frontiersin.org/articles/10.3389/fphy.2021.759005/full#supplementary-material

REFERENCES

1. Weltmann K-D, Von Woedtke T Plasma Medicine-Current State of Research and Medical Application. *Plasma Phys Control Fusion* (2017) 59:014031–41. doi:10.1088/0741-3335/59/1/014031

2. Khlyustova A, Labay C, Machala Z, Ginebra M-P, Canal C Important Parameters in Plasma Jets for the Production of RONS in Liquids for Plasma Medicine: A Brief Review. *Front Chem Sci Eng* (2019) 13:238–52. doi:10.1007/s11705-019-1801-8

3. Von Woedtke T, Schmidt A, Bekeschus S, Wende K, Weltmann K-D Plasma Medicine: A Field of Applied Redox Biology. *In Vivo* (2019) 33:1011–26. doi:10.21873/invivo.11570

4. Stratmann B, Costea T-C, Nolte C, Hiller J, Schmidt J, Reindel J, et al. Effect of Cold Atmospheric Plasma Therapy vs Standard Therapy Placebo on Wound Healing in Patients with Diabetic Foot Ulcers. *JAMA Netw Open* (2020) 3: e2010411. doi:10.1001/jamanetworkopen.2020.10411

5. Zhang W, Hu X, Shen Q, Xing D Mitochondria-specific Drug Release and Reactive Oxygen Species Burst Induced by Polyprodrug Nanoreactors Can Enhance Chemotherapy. *Nat Commun* (2019) 10:1704. doi:10.1038/s41467-019-09566-3

6. Tang ZM, Liu YY, Ni DL, Zhou JJ, Zhang M, Zhao PR, et al. Biodegradable Nanoprodrugs: "Delivering" ROS to Cancer Cells for Molecular Dynamic Therapy. *Adv Mater* (2020) 32:e1904011. doi:10.1002/adma.201904011

7. Agostinis P, Berg K, Cengel KA, Foster TH, Girotti AW, Gollnick SO, et al. Photodynamic Therapy of Cancer: an Update. *CA: A Cancer J Clinicians* (2011) 61:250–81. doi:10.3322/caac.20114

8. Graves DB Mechanisms of Plasma Medicine: Coupling Plasma Physics, Biochemistry, and Biology. *IEEE Trans Radiat Plasma Med Sci* (2017) 1: 281–92. doi:10.1109/trpms.2017.2710880

9. Reuter S, Von Woedtke T, Weltmann KD The kINPen-A Review on Physics and Chemistry of the Atmospheric Pressure Plasma Jet and its Applications. *J Phys D-Applied Phys* (2018) 51. doi:10.1088/1361-6463/aab3ad

10. Gay-Mimbrera J, García MC, Isla-Tejera B, Rodero-Serrano A, García-Nieto AV, Ruano J Clinical and Biological Principles of Cold Atmospheric Plasma Application in Skin Cancer. *Adv Ther* (2016) 33:894–909. doi:10.1007/s12325-016-0338-1

11. Liedtke KR, Bekeschus S, Kaeding A, Hackbarth C, Kuehn J-P, Heidecke C-D, et al. Non-thermal Plasma-Treated Solution Demonstrates Antitumor Activity against Pancreatic Cancer Cells *In Vitro* and *In Vivo*. *Sci Rep* (2017) 7:8319. doi:10.1038/s41598-017-08560-3

12. Liedtke KR, Freund E, Hackbarth C, Heidecke C-D, Partecke L-I, Bekeschus S A Myeloid and Lymphoid Infiltrate in Murine Pancreatic Tumors Exposed to Plasma-Treated Medium. *Clin Plasma Med* (2018) 11:10–7. doi:10.1016/j.cpme.2018.07.001

13. Bekeschus S, Schmidt A, Weltmann K-D, Von Woedtke T The Plasma Jet kINPen - A Powerful Tool for Wound Healing. *Clin Plasma Med* (2016) 4: 19–28. doi:10.1016/j.cpme.2016.01.001

14. Bernhardt T, Semmler ML, Schäfer M, Bekeschus S, Emmert S, Boeckmann L. Plasma Medicine: Applications of Cold Atmospheric Pressure Plasma in Dermatology. *Oxid Med Cel Longev* (2019) 2019:3873928. doi:10.1155/2019/3873928

15. Schmidt A, Von Woedtke T, Vollmar B, Hasse S, Bekeschus S Nrf2 Signaling and Inflammation Are Key Events in Physical Plasma-Spurred Wound Healing. *Theranostics* (2019) 9:1066–84. doi:10.7150/thno.29754

16. Lackmann J-W, Bandow JE Inactivation of Microbes and Macromolecules by Atmospheric-Pressure Plasma Jets. *Appl Microbiol Biotechnol* (2014) 98: 6205–13. doi:10.1007/s00253-014-5781-9

17. Jablonowski H, Hänsch MAC, Dünnbier M, Wende K, Hammer MU, Weltmann K-D, et al. Plasma Jet's Shielding Gas Impact on Bacterial Inactivation. *Biointerphases* (2015) 10:029506. doi:10.1116/1.4916533

18. Matthes R, Jablonowski L, Koban I, Quade A, Hübner N-O, Schlueter R, et al. *In Vitro* treatment of Candida Albicans Biofilms on Denture Base Material with Volume Dielectric Barrier Discharge Plasma (VDBD) Compared with Common Chemical Antiseptics. *Clin Oral Invest* (2015) 19:2319–26. doi:10.1007/s00784-015-1463-y

19. Duske K, Koban I, Kindel E, Schröder K, Nebe B, Holtfreter B, et al. Atmospheric Plasma Enhances Wettability and Cell Spreading on Dental Implant Metals. *J Clin Periodontol* (2012) 39:400–7. doi:10.1111/j.1600-051x.2012.01853.x

20. Jablonowski L, Koban I, Berg MH, Kindel E, Duske K, Schröder K, et al. Elimination of E. Faecalis by a New Non-Thermal Atmospheric Pressure Plasma Handheld Device for Endodontic Treatment. A Preliminary Investigation. *Plasma Process. Polym* (2013) 10:499–505. doi:10.1002/ppap.201200156

21. Duske K, Jablonowski L, Koban I, Matthes R, Holtfreter B, Sckell A, et al. Cold Atmospheric Plasma in Combination with Mechanical Treatment Improves Osteoblast Growth on Biofilm Covered Titanium Discs. *Biomaterials* (2015) 52:327–34. doi:10.1016/j.biomaterials.2015.02.035

22. Hartwig S, Doll C, Voss JO, Hertel M, Preissner S, Raguse JD Treatment of Wound Healing Disorders of Radial Forearm Free Flap Donor Sites Using Cold Atmospheric Plasma: A Proof of Concept. *J Oral Maxillofac Surg* (2017) 75:429–35. doi:10.1016/j.joms.2016.08.011

23. Bruggeman PJ, Kushner MJ, Locke BR, Gardeniers JGE, Graham WG, Graves DB, et al. Plasma-liquid Interactions: a Review and Roadmap. *Plasma Sourc Sci. Technol.* (2016) 25:053002. doi:10.1088/0963-0252/25/5/053002

24. Bruno G, Heusler T, Lackmann J-W, Von Woedtke T, Weltmann K-D, Wende K Cold Physical Plasma-Induced Oxidation of Cysteine Yields Reactive Sulfur Species (RSS). *Clin Plasma Med* (2019) 14:100083. doi:10.1016/j.cpme.2019.100083

25. Brandenburg R Dielectric Barrier Discharges: Progress on Plasma Sources and on the Understanding of Regimes and Single Filaments. *Plasma Sourc Sci. Technol.* (2017) 26:053001. doi:10.1088/1361-6595/aa6426

26. Bruggeman PJ, Iza F, Brandenburg R Foundations of Atmospheric Pressure Non-equilibrium Plasmas. *Plasma Sourc Sci. Technol.* (2017) 26:123002. doi:10.1088/1361-6595/aa97af

27. Takai E, Kitamura T, Kuwabara J, Ikawa S, Yoshizawa S, Shiraki K, et al. Chemical Modification of Amino Acids by Atmospheric-Pressure Cold Plasma in Aqueous Solution. *J Phys D: Appl Phys* (2014) 47:285403. doi:10.1088/0022-3727/47/28/285403

28. Lackmann JW, Baldus S, Steinborn E, Edengeiser E, Kogelheide F, Langklotz S, et al. A Dielectric Barrier Discharge Terminally Inactivates RNase A by Oxidizing Sulfur-Containing Amino Acids and Breaking Structural Disulfide Bonds. *J Phys D-Applied Phys* (2015) 48. doi:10.1088/0022-3727/48/49/494003

29. Verlackt CCW, Van Boxem W, Dewaele D, Lemière F, Sobott F, Benedikt J, et al. Mechanisms of Peptide Oxidation by Hydroxyl Radicals: Insight at the Molecular Scale. *J Phys Chem C* (2017) 121:5787–99. doi:10.1021/acs.jpcc.6b12278

30. Nasri Z, Memari S, Wenske S, Clemen R, Martens U, Delcea M, et al. Singlet Oxygen-Induced Phospholipase A2 Inhibition: a Major Role for Interfacial Tryptophan Dioxidation. *Eur Chem J* (2021) 27(59):14702–10. doi:10.1002/chem.202102306

31. Maheux S, Frache G, Thomann JS, Clément F, Penny C, Belmonte T, et al. Small Unilamellar Liposomes as a Membrane Model for Cell Inactivation by Cold Atmospheric Plasma Treatment. *J Phys D: Appl Phys* (2016) 49:344001. doi:10.1088/0022-3727/49/34/344001

32. Yusupov M, Wende K, Kupsch S, Neyts EC, Reuter S, Bogaerts A Effect of Head Group and Lipid Tail Oxidation in the Cell Membrane Revealed through Integrated Simulations and Experiments. *Sci Rep* (2017) 7:5761. doi:10.1038/s41598-017-06412-8

33. Striesow J, Lackmann J-W, Ni Z, Wenske S, Weltmann K-D, Fedorova M, et al. Oxidative Modification of Skin Lipids by Cold Atmospheric Plasma (CAP): A Standardizable Approach Using RP-LC/MS2 and DI-ESI/MS2. *Chem Phys Lipids* (2020) 226:104786. doi:10.1016/j.chemphyslip.2019.104786

34. Schmidt A, Bekeschus S Redox for Repair: Cold Physical Plasmas and Nrf2 Signaling Promoting Wound Healing. *Antioxidants (Basel)* (2018) 7. doi:10.3390/antiox7100146

35. Muzumdar S, Hiebert H, Haertel E, Ben-Yehuda Greenwald M, Bloch W, Werner S, et al. Nrf2-Mediated Expansion of Pilosebaceous Cells Accelerates Cutaneous Wound Healing. *Am J Pathol* (2019) 189:568–79. doi:10.1016/j.ajpath.2018.11.017

36. Schmidt A, Bekeschus S, Jarick K, Hasse S, Von Woedtke T, Wende K. Cold Physical Plasma Modulates P53 and Mitogen-Activated Protein Kinase Signaling in Keratinocytes. *Oxid Med Cel Longev* (2019) 2019:7017363. doi:10.1155/2019/7017363

37. Jablonowski H, Bussiahn R, Hammer MU, Weltmann K-D, Von Woedtke T, Reuter S Impact of Plasma Jet Vacuum Ultraviolet Radiation on Reactive Oxygen Species Generation in Bio-Relevant Liquids. *Phys Plasmas* (2015) 22: 122008. doi:10.1063/1.4934989

38. Laroussi M, Dobbs FC, Wei Z, Doblin MA, Ball LG, Moreira KR, et al. Decontamination of Water by Excimer UV Radiation. *IEEE Trans Plasma Sci* (2002) 30:1501–3. doi:10.1109/tps.2002.804208

39. Brandenburg R, Lange H, Von Woedtke T, Stieber M, Kindel E, Ehlbeck J, et al. Antimicrobial Effects of UV and VUV Radiation of Nonthermal Plasma Jets. *IEEE Trans Plasma Sci* (2009) 37:877–83. doi:10.1109/tps.2009.2019657

40. Schneider S, Lackmann J-W, Ellerweg D, Denis B, Narberhaus F, Bandow JE, et al. The Role of VUV Radiation in the Inactivation of Bacteria with an Atmospheric Pressure Plasma Jet. *Plasma Process. Polym* (2012) 9:561–8. doi:10.1002/ppap.201100102

41. Judée F, Wattieaux G, Merbahi N, Mansour M, Castanié-Cornet MP The Antibacterial Activity of a Microwave Argon Plasma Jet at Atmospheric Pressure Relies Mainly on UV-C Radiations. *J Phys D: Appl Phys* (2014) 47:405201. doi:10.1088/0022-3727/47/40/405201

42. Lange H, Foest R, Schafer J, Weltmann K-D Vacuum UV Radiation of a Plasma Jet Operated with Rare Gases at Atmospheric Pressure. *IEEE Trans Plasma Sci* (2009) 37:859–65. doi:10.1109/tps.2009.2019982

43. Bahre H, Lange H, Schulz-Von Der Gathen V, Foest R. Vacuum Ultraviolet (VUV) Emission of an Atmospheric Pressure Plasma Jet (M-APPJ) Operated in Helium-Oxygen Mixtures in Ambient Air. *Acta Technica* (2011) 56.

44. Yurkova I, Shadyro O, Kisel M, Brede O, Arnhold J Radiation-induced Free-Radical Transformation of Phospholipids: MALDI-TOF MS Study. *Chem Phys Lipids* (2004) 132:235–46. doi:10.1016/j.chemphyslip.2004.08.006

45. Corre I, Niaudet C, Paris F Plasma Membrane Signaling Induced by Ionizing Radiation. *Mutat Research/Reviews Mutat Res* (2010) 704:61–7. doi:10.1016/j.mrrev.2010.01.014

46. Rastogi RP, RichaKumar A, Kumar A, Tyagi MB, Sinha RP. Molecular Mechanisms of Ultraviolet Radiation-Induced DNA Damage and Repair. *J Nucleic Acids* (2010) 2010:592980. doi:10.4061/2010/592980

47. Islam MT Radiation Interactions with Biological Systems. *Int J Radiat Biol* (2017) 93:487–93. doi:10.1080/09553002.2017.1286050

48. Lalande M, Schwob L, Vizcaino V, Chirot F, Dugourd P, Schlathölter T, et al. Direct Radiation Effects on the Structure and Stability of Collagen and Other Proteins. *Chembiochem* (2019) 20:2972–80. doi:10.1002/cbic.201900202

49. Mikkelsen RB, Wardman P Biological Chemistry of Reactive Oxygen and Nitrogen and Radiation-Induced Signal Transduction Mechanisms. *Oncogene* (2003) 22:5734–54. doi:10.1038/sj.onc.1206663

50. Pattison DI, Davies MJ *Actions of Ultraviolet Light on Cellular Structures*. Birkhaeuser, Basel: EXS (2006). p. 131–57.

51. Pattison DI, Rahmanto AS, Davies MJ Photo-oxidation of Proteins. *Photochem Photobiol Sci* (2012) 11:38–53. doi:10.1039/c1pp05164d

52. Von Woedtke T, Jülich W-D, Thal S, Diederich M, Stieber M, Kindel E Antimicrobial Efficacy and Potential Application of a Newly Developed Plasma-Based Ultraviolet Irradiation Facility. *J Hosp Infect* (2003) 55: 204–11. doi:10.1016/s0195-6701(03)00290-1

53. Laroussi M, Leipold F Evaluation of the Roles of Reactive Species, Heat, and UV Radiation in the Inactivation of Bacterial Cells by Air Plasmas at Atmospheric Pressure. *Int J Mass Spectrom* (2004) 233:81–6. doi:10.1016/j.ijms.2003.11.016

54. Lackmann J-W, Bruno G, Jablonowski H, Kogelheide F, Offerhaus B, Held J, et al. Nitrosylation vs. Oxidation - How to Modulate Cold Physical Plasmas for Biological Applications. *PLoS One* (2019) 14:e0216606. doi:10.1371/journal.pone.0216606

55. Wende K, Bruno G, Lalk M, Weltmann K-D, Von Woedtke T, Bekeschus S, et al. On a Heavy Path - Determining Cold Plasma-Derived Short-Lived Species Chemistry Using Isotopic Labelling. *RSC Adv* (2020) 10:11598–607. doi:10.1039/c9ra08745a

56. Sremački I, Bruno G, Jablonowski H, Leys C, Nikiforov AY, Wende K Influence of Aerosol Injection on the Liquid Chemistry Induced by an RF Argon Plasma Jet. *Plasma Sources Sci. Technol.* (2021) 30(9). doi:10.1088/1361-6595/abe176

57. Pikal-Cleland KA, Cleland JL, Anchordoquy TJ, Carpenter JF. Effect of glycine on pH Changes and Protein Stability during Freeze-Thawing in Phosphate Buffer Systems. *J Pharm Sci* (2002) 91:1969–79. doi:10.1002/jps.10184

58. Jacobi U, Kaiser M, Toll R, Mangelsdorf S, Audring H, Otberg N, et al. Porcine Ear Skin: an *In Vitro* Model for Human Skin. *Skin Res Technol* (2007) 13: 19–24. doi:10.1111/j.1600-0846.2006.00179.x

59. Myers B, Ranieri P, Smirnova T, Hewitt P, Peterson D, Quesada MH, et al. Measuring Plasma-Generated center Dot OH and O Atoms in Liquid Using EPR Spectroscopy and the Non-selectivity of the HTA Assay. *J Phys D-Applied Phys* (2021) 54. doi:10.1088/1361-6463/abd9a6

60. Shen X, Kolluru GK, Yuan S, Kevil CG Measurement of H2S *In Vivo* and *In Vitro* by the Monobromobimane Method. *Methods Enzymol* (2015) 554:31–45. doi:10.1016/bs.mie.2014.11.039

61. Foest R, Kindel E, Lange H, Ohl A, Stieber M, Weltmann K-D RF Capillary Jet - a Tool for Localized Surface Treatment. *Contrib Plasma Phys* (2007) 47: 119–28. doi:10.1002/ctpp.200710017

62. Reuter S, Winter J, Schmidt-Bleker A, Schroeder D, Lange H, Knake N, et al. Atomic Oxygen in a Cold Argon Plasma Jet: TALIF Spectroscopy in Ambient Air with Modelling and Measurements of Ambient Species Diffusion. *Plasma Sourc Sci Tech* (2012) 21:024005.%&

63. Abedinzadeh Z, Gardes-Albert M, Ferradini C Kinetic Study of the Oxidation Mechanism of Glutathione by Hydrogen Peroxide in Neutral Aqueous Medium. *Can J Chem* (1989) 67:1247–55. doi:10.1139/v89-190

64. Luo D, Smith SW, Anderson BD Kinetics and Mechanism of the Reaction of Cysteine and Hydrogen Peroxide in Aqueous Solution. *J Pharm Sci* (2005) 94: 304–16. doi:10.1002/jps.20253

65. Enescu M, Cardey B Mechanism of Cysteine Oxidation by a Hydroxyl Radical: a Theoretical Study. *Chem Eur J Chem Phys* (2006) 7:912–9. doi:10.1002/cphc.200500585

66. Gupta V, Carroll KS Sulfenic Acid Chemistry, Detection and Cellular Lifetime. *Biochim Biophys Acta (Bba) - Gen Subjects* (2014) 1840:847–75. doi:10.1016/j.bbagen.2013.05.040

67. Chauvin J-PR, Pratt DA On the Reactions of Thiols, Sulfenic Acids, and Sulfinic Acids with Hydrogen Peroxide. *Angew Chem Int Ed* (2017) 56:6255–9. doi:10.1002/anie.201610402

68. Stans MH *Bond Dissociation Energies in Simple Molecules*NIST Special Publication 1 %6, 58 %& (1970).

69. Wende K, Bekeschus S, Schmidt A, Jatsch L, Hasse S, Weltmann KD, et al. Risk Assessment of a Cold Argon Plasma Jet in Respect to its Mutagenicity. *Mutat Research/Genetic Toxicol Environ Mutagenesis* (2016) 798-799:48–54. doi:10.1016/j.mrgentox.2016.02.003

70. Schmidt A, Woedtke TV, Stenzel J, Lindner T, Polei S, Vollmar B, et al. One Year Follow-Up Risk Assessment in SKH-1 Mice and Wounds Treated with an Argon Plasma Jet. *Int J Mol Sci* (2017) 18. doi:10.3390/ijms18040868

71. Bekeschus S, Schmidt A, Kramer A, Metelmann H-R, Adler F, Von Woedtke T, et al. High Throughput Image Cytometry Micronucleus Assay to Investigate the Presence or Absence of Mutagenic Effects of Cold Physical Plasma. *Environ Mol Mutagen* (2018) 59:268–77. doi:10.1002/em.22172

72. Linxiang L, Abe Y, Nagasawa Y, Kudo R, Usui N, Imai K, et al. An HPLC Assay of Hydroxyl Radicals by the Hydroxylation Reaction of Terephthalic Acid. *Biomed Chromatogr* (2004) 18:470–4. doi:10.1002/bmc.339